Mine Water Environ (2017) 36:443–451
DOI 10.1007/s10230-017-0433-9

TECHNICAL COMMUNICATION

Experimental Simulation of Fault Water Inrush Channel Evolution in a Coal Mine Floor

Shichuan Zhang[1] · Weijia Guo[1] · Yangyang Li[1] · Wenbin Sun[1] · Dawei Yin[1]

Received: 30 December 2015 / Accepted: 18 January 2017 / Published online: 27 February 2017

Abstract Mine water inrush is very common in China and can cause hysteresis and severe damage. The entire process of crack formation, concealed fault propagation, and evolution of a water inrush channel with high pressure water directly beneath the mine floor was physically simulated based on fluid–solid coupling mechanics and solid materials research. Activated materials were used to simulate fault damaged rock, including soybeans, sand, Vaseline, and calcium carbonate. The results indicate that water channels are mainly caused by the connection between tectonic rock zones and coal floor cracks, which are the direct cause for water inrush. Furthermore, the lagging water inrush mechanism from the coal floor in a confined water body under both a stress field and a seepage field were revealed. The formation of the water inrush path with temporal and spatial variations was analyzed by interpreting the monitoring data and phenomena. The data showed that the floor stress in front of the working face increased and was affected by the abutment pressure, and that floor stress under the mined-out area began to decrease simultaneously. The stress of the upper wall showed a drastic drop while the stress of the footwall continued to decline and then stabilized after the water inrush. This work provides new approaches and knowledge for research on deep mining water inrush structures.

Keywords Rock mechanics · Similar materials · Stress monitoring · Total process

Introduction

Coal mining is seriously affected as faults disturbed by mining become water conducting passages. Many floor water inrushes have occurred in China, and the number of national coal mine inrush disasters has increased (Wu et al. 2013a). There is still no unified standard to classify coal mine inrush events (Chao and Gong 2011) because different types of water inrush have different mechanisms. Water inrush events are controlled by many complex factors, such as the state of the coal seam and the geologic structure (Liu 2009). Furthermore, as mining depths and mining intensity increase, the encountered hydrogeological conditions have become more complicated (James et al. 2014). Regardless of the type of floor water inrush, the main causes are the deformation, displacement, and failure of the floor plate due to the combined effects of lithostatic and hydrostatic pressure. Therefore, understanding the evolution and mechanism of water inrush channels could be the key to preventing inrush events.

Water inrush events have been studied based on both theoretical analysis and numerical simulation (Zhang and Shen 2004). With respect to theoretical analysis, the inrush mechanism of the complete floor and floor affected by fault

S. Zhang and W. Guo contributed equally to this work.

Electronic supplementary material The online version of this article (doi:10.1007/s10230-017-0433-9) contains supplementary material, which is available to authorized users.

✉ Shichuan Zhang
373260186@qq.com

✉ Yangyang Li
1161826089@qq.com

[1] State Key Laboratory of Mining Disaster Prevention and Control, Shandong University of Science and Technology, Shandong 266590, China

structures was determined by an elastic–plastic theory and a statistical method (Ministry of Coal Industry 2009). A series of implementation evaluations were established for evaluating and predicting inrush, such as an Analytischen Hierarchie Prozesses model and an evaluation model based on a support vector machine, which provided theoretical evidence for forecasting floor water inrush (Wu et al. 2009, 2013b, 2015). Bukowski (2011) established a risk assessment system, which classifies mine shafts with respect to the risk of a water hazard. Also, a secondary fuzzy comprehensive evaluation system (Wang et al. 2012) was constructed to assess the risk of floor water inrush in coal mines. Evaluations of engineering practices were conducted with hydrogeological data from six mining faces in China, and the results were consistent with observations.

The Hybrid Finite Element Mixing Cell method (Wildemeersch et al. 2010) is a flexible modeling technique particularly suited to mining problems, which makes it useful for managing mine closure issues such as groundwater rebound and water inrush. Many scholars have used software to simulate crack propagation and the floor water inrush process (Li et al. 2013; Lu and Wang 2015; Wang et al. 2011).

The physical simulation and observation of the water channel evolution process is an important approach in researching water inrush from a fault, and can make up for the deficiencies of the above stated methods. Physical similitude modeling studies the laws of nature by making use of the similarity and analogy of objects. For example, Wang et al. (2010) used a test platform to simulate two different water inrush processes in a collapsed column. An extendable testing system (Li et al. 2014) modeling water inrush was developed to investigate the F4-4 fault at the undersea tunnel in Jiaozhou Bay near Qingdao. Liu (2009) developed a physical modelling test system similar to the deep-mining confined water inrush mechanism, which could realize the stress, deformation, and destruction process of the rock mass under the complicated joint action of the stress of water pressure and mining, and simulated and tested micro–macro migration rules. Zhou et al. (2006) designed and developed a salt rock crack penetrating-dissolving coupling test device, and carried out experimental studies of salt rock crack penetrating-dissolving coupling process.

Sun and Zhang (2015a) developed appropriate fluid–solid coupling materials and proposed materials for simulating coal mine floor rock. While this work presented a solid foundation to solve the instability problems involved in coupling fluids and porous media, their chosen materials could not simulate fault activation. Thus, the formation and evolution of inrush channels remain to be demonstrated in visual experimental research.

Modeling test systems have several problems, including that it is difficult for a test stand to meet all comprehensive requirements for factors such as rigidity, intensity, leak tightness, and visualization, and the test stand size and structure is fixed, which means that one cannot conduct a test with different size requirements. Also, the model body is usually filled with a single material, which only allows two-dimensional simulation and lacks the capability for an analog simulation of complicated geological conditions. However, in this research, various materials with different hydrological characteristics were used to simulate the rock surrounding the floor and the fault fluid–structure interaction, allowing us to study the evolution of water inrush during mining. A fault activation inrush test model was also established. A floor water invasion simulation testing system, designed at the Shandong University of Science and Technology (China), was used for visual observation of spatiotemporal evolution of inrush through a simulated mine floor under high water pressure by monitoring structural stress, fault deformation, and breakage.

Test Conditions

Test Equipment

The floor water inrush simulation testing system (Sun and Zhang 2015b) designed at the Shandong University of Science and Technology was used in this study. The test stand operation consists of:

1. Filling the materials test-bed with materials that simulate the coal and rock, simulating the proportions of the actual geological structure, and installing corresponding stress and pore water pressure sensors.
2. Starting the hydraulic pressure servo-loading system, and increasing the horizontal and vertical loads gradually until it reaches the designed load.
3. Filling the test bed with water until it reaches the desired water pressure.
4. Excavating the simulated coal seam to mimic the actual mining technology, until the confined water passes through the inrush channel.

Model Design

Similarity Criteria Analysis

This experiment was conducted based on the actual geological conditions of a coal mine in the Jibei mining area, where the mining depth is 850 m (below the surface), the coal seam thickness is 2 m, the base plate thickness is 22 m,

and the aquifer water pressure is 3.38 MPa. By geologic structure detection, there is a buried structure in the range of the working face with a dip angle of 68° and a length of 36 m. There is a fault around the stop line, with a dip angle of 70° and fall head of 5 m, which is protected by a 15 m wide pillar. Rock cores revealed that the fault fracture zone had a granulated fracture texture, with the lithological characters of mudstone. The upper wall and footwall were both fractured. The water flow of the drilling hole was 2.5–3.0 m^3/h, and the fault has abundant water, with excellent water conductivity.

Supplementary Table 1 presents the physical properties of the Jibei strata. In addition to satisfying the requirements of solid deformation and permeability, the physical and hydraulic properties of the model materials had to simulate the physical and hydraulic properties of the actual strata. Based on the physical simulation test conditions and a theoretical analysis, a similar model was designed based on the documented mining conditions and equipment size, with a similarity ratio of 1:100. Based on the π theorem of the Similarity Three Theorem (Hu et al. 2007), the main similarity parameters can be derived as follows: the geometric similarity was 1/100; the time similarity was 1/10; the bulk density similarity was 1/1.5; the elasticity modulus similarity coefficient was 1/150; and the permeability coefficient similarity was 1/10.

Selection of Similar Materials

The roof and coal seam were simulated using a proportioned mixture of fluvial sand, gypsum, and calcium carbonate chosen to mimic the properties of each. The floor materials were similar non-hydrophilic materials, again created with proportioned amounts of fluvial sand, calcium carbonate, and paraffin wax (Sun and Zhang 2015a).

The fault simulation materials also play an important role in revealing the mechanism of induced water inrush and the evolution of a water channel caused by fault activation. With a mean diameter of 8 mm, soybeans were selected as the fault simulation material. Soybeans release energy as they swell after absorbing water, generating destructive power that is locally significant in a confined space. Compared with cement, soybeans are more activated by water immersion than other materials, and can indirectly simulate the hydraulic pressure of the surrounding rock. To create the fault simulation material, the soybeans were added to river sand (about 0.4–0.6 mm), light calcium carbonate, and high strength gypsum. The ratio of the four types of materials was 8:6:1:2 (Supplementary Fig. 1).

An experiment was conducted to assess the feasibility of the material and potential problems. In making the fault rupture simulation specimens, the effect of extrusion fracturing of the floor rock was examined. The fault rupture simulation specimen was made up of two materials, namely, a solid–liquid coupling material and a fault simulation material. The interior of the specimen was a cylindrical interlayer (20 mm in diameter, 70 mm in height), made of the fault materials. The external portion of the specimen (50 mm in diameter, 100 mm in height) was made of the solid–liquid coupling (Fig. 1). This study simulated three types of floor rock: limestone, mudstone, and siltstone. As shown in Table 1, every factor was used to test the materials, and seven testing schemes (D1–D7) were identified. The fault rupture simulation specimens were tested by water immersion.

Loading Conditions Sensors Arrangement

The model was designed to be similar to the actual mining conditions. The rock mass was made of siltstone below the coal floor, which changes from an elastic state to a latent plastic state at −850 m (He 2005). The average bulk density of the overlying strata in the coal measure strata was taken to be 25 kN/m^3. Based on the similarity coefficient, the appropriate horizontal load of the model was calculated to be 0.196 MPa. The conditions are, of course, restricted by the size of the simulation test system, so the appropriate imposed water pressure at the floor was calculated to be 0.03 MPa. Under this geological condition, if the shear power of the shear surface above the buried structure is greater than that of the rock mass, the floor will fail.

The servo-loading system of the test bed provided the applied stress. The corresponding water pressure was provided by the hydraulic loading system. The model of floor crack propagation is shown in Fig. 2.

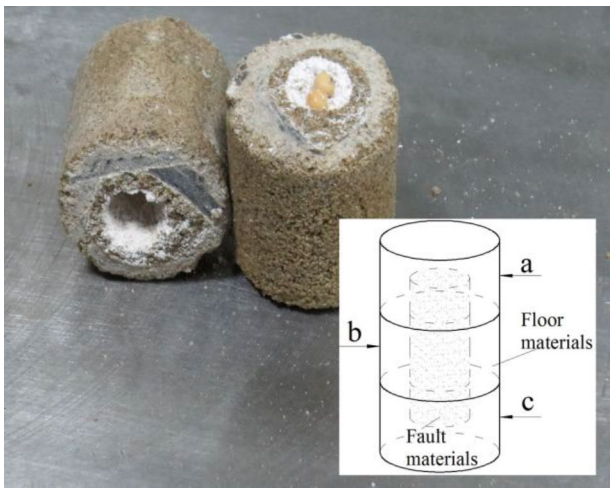

Fig. 1 Fault rupture of simulation specimens

Table 1 Proportion schemes of similar material

Design	External material			Interior material	Remark
	a	b	c		
D1	Limestone	Mudstone	Siltstone	Fault material	D1–D7 Soaking
D2	Limestone	Siltstone	Mudstone	Fault material	D1–D3 different external material
D3	Mudstone	Limestone	Siltstone	Fault material	
D4	Siltstone	Siltstone	Siltstone	Fault material	D4–D6 uniform external materials
D5	Mudstone	Mudstone	Mudstone	Fault material	
D6	Limestone	Limestone	Limestone	Fault material	
D7	Limestone	Limestone	Limestone	Floor material	D7 Contrast test

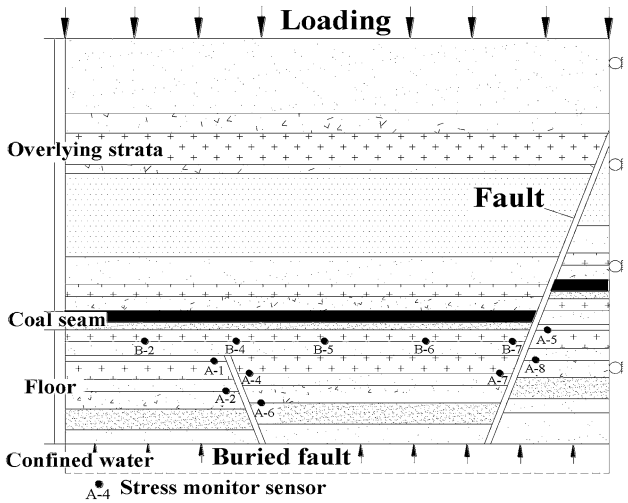

Fig. 2 Model of floor crack propagation

The stress changes near the floor and the fault during mining was monitored using a BX-1 sensor, which has a maximum observed value of 0.8 MPa. The experimental data were collected using a DH-3816N static strain measurement system, at a sampling rate of 60 points per second, and a strain sensitivity coefficient of about 1.0–3.0. Sensor placement and the multivariate data acquisition system are shown in Supplementary Fig. 2.

Model Layout

The experimental steps were as follows:

1. Lay the heated mixed material on the floor of the test bed, so that the compacted layer reaches the design elevation.
2. Add quantitative mica powder to the interface between the layers. Place eight stress sensors on the design site with four stress sensors below the floor mudstone at a distance of 15 cm from each other. Two stress sensors are put on each side of the fault. The distance between the stress sensors and the fault boundary is 2 cm.
3. Cut the rock material according to the fault location, and then, add the fault materials and immobilize them.
4. Install the organic glass (fiberglass) on the bilateral section of the device. The transverse loading mechanism then imposes transverse stress to the floor by the side plate.
5. Two days later, induce vertical and horizontal loading stress, and set the hydraulics and loading.
6. Excavate the coal and collect the data. Supplementary Fig. 3 shows the test model after the experiment was completed.

Error Analysis

1. Errors of the boundary conditions: Unmatched boundary conditions would reduce the similarity between the systems, which would create experimental error. In this experiment, a smooth steel plate was placed between the test stand and similar materials to reduce frictional resistance and decrease boundary conditions errors.
2. Errors of the composition of similar materials: Moisture variability would lead to material strength changes, as well as errors in similarity between the model and actual mechanical conditions. In addition, variability in the materials, such as grading of the river sand or impurities, could cause deviations in the strength of similar materials. To avoid these problems, the model was made strictly following the required temperature and moisture conditions.
3. Observation errors: The smaller the scale of the model, the greater the impact of observational errors on the experimental result. Generally, geometric similarity scales can be selected between 1:50 and 1:200. In this test, it was 1:100.

Results and Discussion

Water Inrush Channel: Effect of Cracks in the Fault Materials

The damage of the D5 specimen appeared after soaking for 7 h; the rupture pattern is shown in Fig. 3a. The main

failure mode caused longitudinal perforation damage as well as transverse micro-cracks. After soaking for 15 h, D4 and D6 were damaged, like the D5 specimen. Soybean expansion after soaking caused the mudstone specimen to rupture. The failure modes of the D1, D2, and D3 specimens are shown in Fig. 3b, c. After soaking for 8 h, the mudstone section of the specimen ruptured first; the main failure mode was transverse perforation along with small longitudinal micro-cracks. The transverse fissure first appeared in the middle of the D1 specimen during the influx of water. Then, the specimen fractured; the damage was associated with the evolution of vertical fissures. The middle of the D2 and D3 specimens were siltstone and limestone and were not damaged after soaking for 8 h. The broken ends of the mudstone were obvious, and the failure mode of the ends was transverse perforation. Rupture failure did not occur in the D7 specimen.

The results show that in floor strata of different lithologies, the cracks first occurred in the strata of lower strength. The damage cracks increased in size and magnitude until a large water inrush channel formed. The fault materials can simulate activation over time, and the space effect can indirectly simulate the influence of water pressure on the surrounding rock.

Similar Materials Ratio

According to the above test results, the test design of floor fault extension evolution, and the underground water course model, appropriately similar materials were selected, as shown in Table 2. Physical and hydraulic properties of the model materials are provided in Supplementary Table 2.

Water Inrush Channel Test: Concealed Fault Evolution

During analysis of the test results in this paper, the involved size was the model size. Stress field variations near the mining process fault and the evolution of the fault to form a water inrush channel were examined. The water was stained with blue dye to facilitate the experimental phenomena.

Initial Stress State on Rock Mass Models

After the loading pressure stabilized, the water mark of the confined water guide (the blue area) rose at the floor of the model and can be observed on the test bench opposite (Supplementary Fig. 4). Near the buried structure and the large fault, the height of the confined water guide rise was approximately 6 cm. The natural progressive intrusion

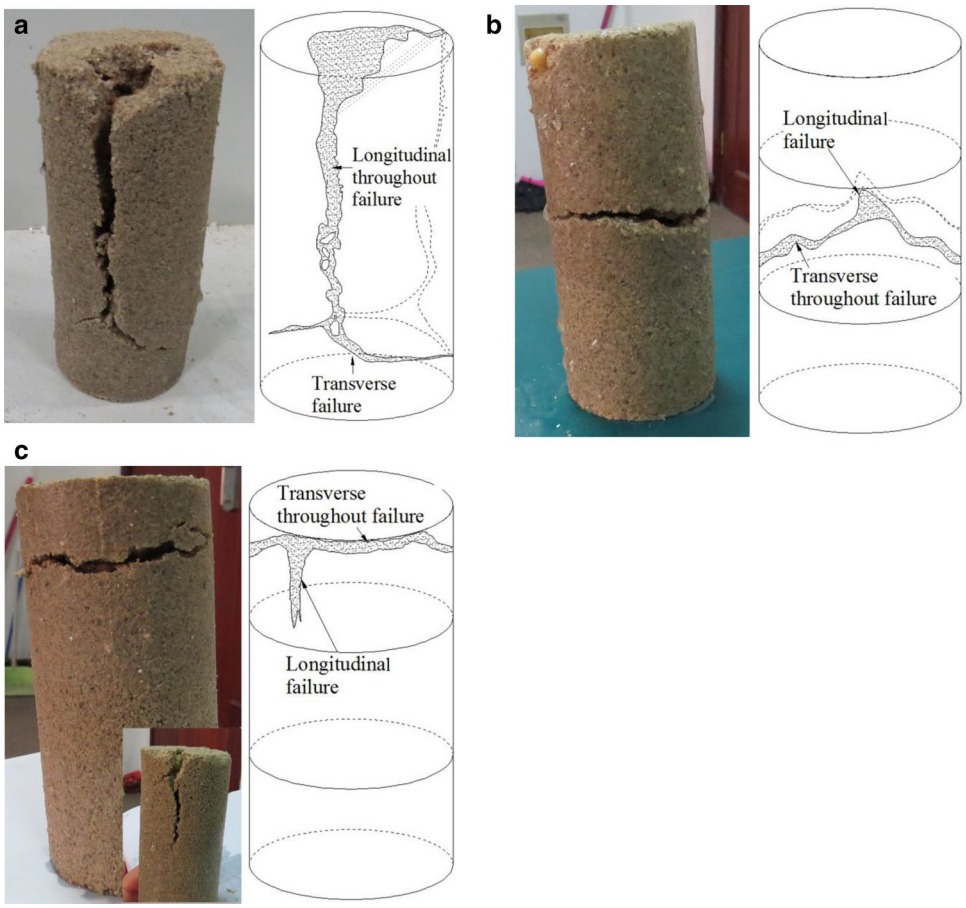

Fig. 3 Different forms of rupture **a** homogeneous failure **b** middle failure **c** two ends failure

height of the confined water along the original geological structure was approximately 3 cm. The results coincided with the "down three zone" theory and show that preexisting fissures in geological structures and guide rise fissures of confined flowing water zones play a significant role in water conductivity.

Fault Activation and Water Inrush Stage

As shown in Fig. 4 and Supplementary Fig. 5, the first roof weighting occurs when the working face advanced to 20 m. Affected by the confined water, the minor fractures of the buried fault were extended and transfixed. Through the organic glass, it can be seen that when the working face advanced to 20 m, cracks in the rock surrounding the fault were dyed blue, and the range increased accordingly. Tension and shear joints appeared in the rock near the fault because of stress concentration, and the joints were arranged like a pinnate; the attitude of the joints was unstable. The status of the fault zone rock mass changed from bonding status to a disconnected status; the permeability was greatly enhanced, and water inrush was easy to induce.

When mined to 25 m, the first roof collapse occurred when the height of the water flow and the end of the buried fault were in the same horizontal position. Various primary fractures developed in the floor and the number of fractures increased slowly. When the mine width reached 30 m, coal floor cracks, including horizontal, vertical, and reticulate cracks, were observed near the buried fault. At the same time, blue confined water gushed out onto the surface of

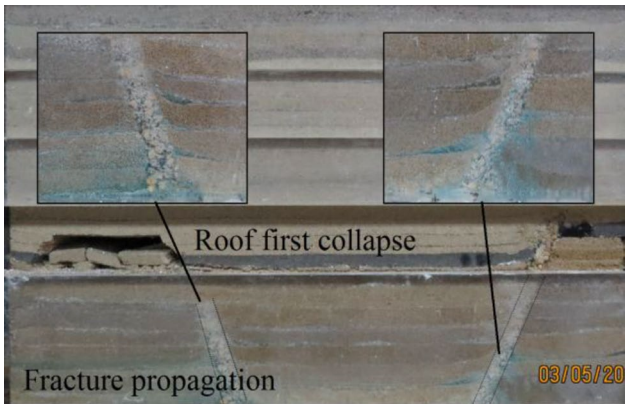

Fig. 4 Water pressure distribution of the entire model

the mined-out floor area, which was located at the top of the buried fault (Supplementary Fig. 6). With more mining, the immediate roof gradually fell and poured out because of the confined water.

As shown in Fig. 5, when mining to 25 m, a smaller water inrush point appeared in the middle of the gob approximately 20 m behind the working face, atop the buried fault. The flow there increased with time, along with a small amount of floor sand. As the inrush channel expanded, the number of inrush points and inrush flow increased. The collapsed rock eventually rushed out, creating a simulated water inrush disaster. "The principle of minimum resistance" can be translated as the shortest distance between two points (i.e. the main water inrush

Table 2 Ratios of similar materials

Rock	Cumulative thickness (cm)	Material ratio (%)			
		River sand	Calcium carbonate	Gypsum	Water
Roof					
Siltstone	18.49	75.00	5.83	2.50	16.67
Limestone	7.91	66.67	10.00	6.67	16.67
Mudstone	7.85	66.67	11.67	5.00	16.67
Conglomerate	15	75.00	5.83	2.50	16.67
Coal					
16 coal	2.01	75.00	5.83	2.50	16.67
		River sand	Calcium carbonate	Paraffin	Regulator
Floor					
Siltstone	7.07	87.00	3.00	5.90	4.10
Mudstone	5.38	84.00	6.00	5.90	4.10
Limestone	3.20	83.00	7.00	3.20	6.80
		River sand	Calcium carbonate	Gypsum	Soybean
Fault					
Filler	2	47.06	35.29	5.88	11.76

point and the end of the buried fault), thus explaining the observed phenomena.

Floor Stress Change Trend

As the working face mined shifted from 15 to 20 m, the floor stress, fracture development, and confined water level dramatically changed (Fig. 6). The B-2 monitoring data prove that the floor stress in front of the working face increased and was affected by abutment pressure; the monitoring stress increment was 0.01 MPa. When the working face was far away (20 m mined), the stress was low and decreased to −0.2 MPa. When the working surface increased from 20 to 40 m, the B-4 stress monitoring value first increased and then decreased, from 0 to 0.025 to −0.2 MPa.

As the working face was mined from 20 to 40 m, the stress at every monitoring point showed obvious fluctuations. Fault activation and water inrush both affect stress, which explains this phenomenon. Figure 6 shows that the areas of increasing stress moved as the working face advanced (40 m mined); the floor stress under the mined-out area decreased simultaneously. As mining proceeded, the stress changes at B-5, B-6, and B-2 showed distinct variation trends due to the impact of the confined water.

Figure 7 shows how the rock surrounding the buried fault stress changed. A-1 and A-2 were close to the confined aquifer and located in the buried fault footwall of A-4 and A-6, and were close to the coal seam in the hanging wall. When the working surface reached 5 m, the monitoring stress of A-1 and A-2 dropped to −0.14 MPa, with the same type of variations. But A-2 showed three fluctuations. When mining reached 40 m, the influence of the water inrush increased the stress at A-1 and A-2, which rose to −0.03 and −0.01 MPa, respectively, while

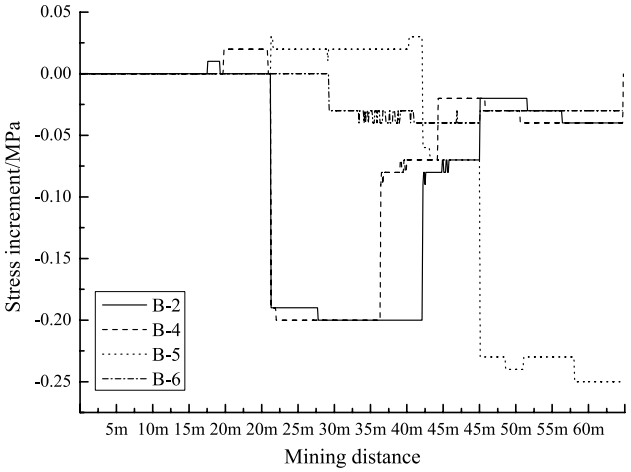

Fig. 6 Floor stress changes in the measured curve

A-4 and A-6 showed distinct variability. When mining reached 45 m, the stress at two sensors declined, and A-4 showed great fluctuations. When it reached 45 to 60 m, water inrush occurred at the working surface, but the stress at A-4 and A-6 maintained a constant value of −0.09 MPa.

As mining proceeded, the floor stress had a short-term unloading, following A-4 and A-6. Significant stress unloading appeared beneath where the coal seam was first mined at A-1 and A-2. The stress changed differently in the hanging wall and the footwall, with greater unloading in the latter. In addition, the sensor near the gob showed an obvious change relative to the sensor close to the aquifer. The monitoring data showed that laminar flow was the main factor influencing stress unloading, and the effect at the footwall was greater than at the hanging wall.

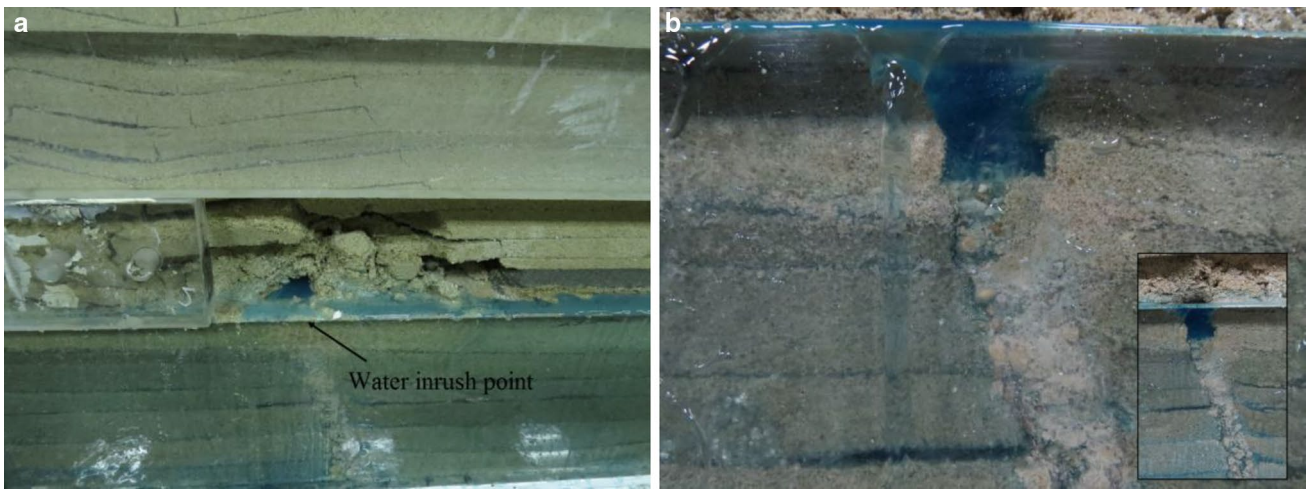

Fig. 5 Formation process of a water inrush channel **a** generating a water inrush channel **b** expansion a water inrush channel

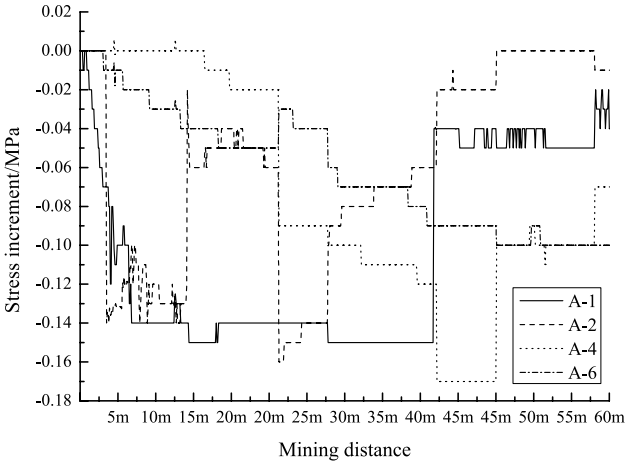

Fig. 7 Measured force curve of small faults

When mining to 20 m, the monitoring data changed after the initial pressure was applied. Combined with the physical experiment, an obvious crack extension phenomenon occurred over the buried fault; thus, faults are a low intensity belt in the rock mass and can be activated by roof movement.

When the working face advanced from 20 to 35 m, the footwall and hanging wall stress data differed. A-2 increased gradually while A-1 remained basically unchanged. The stresses at A-4 and A-6 were reduced and changed similarly. When mining reached 40 m, water inrush occurred in the working face and over the buried fault. Furthermore, the stress data changed dramatically at 40 m. The structurally destroyed level of the floor increased under the influence of the confined water. The mining-induced fissure of the floor fractured, which led to the formation of the water inrush channel.

Conclusions

The testing system's sealing properties, variations in water pressure, flow rate capacity loading, and bidirectional stress loading all realistically simulated floor water inrush under high geostress in a strong seepage environment. Through the transparent organic glass, the spatiotemporal evolution of the water inrush through the mine floor was visually observed.

The fault materials selected simulated the time and space effect of fault activation, which indirectly influenced water pressure in the surrounding rock. Cracks first occurred in the lower strength floor strata, and the cracks gradually increased and widened until a large water inrush channel formed.

Many cracks occurred under the high hydrostatic and lithostatic pressures, which extended and connected inside the concealed structure. When fracture development and extension reached a certain level, the cracks connected to the fracture at the floor of the goaf. An inrush channel, connected to the confined water, was immediately produced, allowing water to inrush over the concealed fault, following "the principle of minimum resistance".

Acknowledgements This research was financially supported by the National Natural Science Foundation of China (Grants 51604167), China Postdoctoral Science Foundation (Grant 2015M572067), Natural Foundation of Shandong Province (ZR2016EEB07), Graduate Innovation Foundation of Shandong University of Science and Technology (SDKDYC170302), and the Taishan Scholar Talent Team Support Plan for Advantaged and Unique Discipline Areas.

References

Aihua L, Peng S, Li X (2009) Development and application of similar physical model experiment system for water inrush mechanism in deep mining. J Rock Mech Eng 28(7):1335–1341 **(Chinese)**

Bukowski P (2011) Water hazard assessment in active shafts in Upper Silesian coal basin mines. Mine Water Environ 30:302–311

Chao X, Gong P (2011) Water disaster types and water control measures of Hanxing coal mine area. P Earth Planet Sci 3:343–348

HE M, Xie H, Peng S, Jiang Y (2005) Study on rock mechanics in deep mining engineering. J Rock Mech Eng 24(16):2803–2812 **(Chinese)**

Hu Y, Zhao Y, Yang D (2007) The study of 3D solid-liquid coupling simulation stope deformation. J Liaoning Tech U 26(4):520–523 **(Chinese)**

James W, LaMoreaux, Wu Q, Zhou W (2014) New development in theory and practice in mine water control in China. Carbonate Evaporite 29:141–145

Li C, Li J, Li Z, Hou D (2013) Establishment of spatiotemporal dynamic model for water inrush spreading processes in underground mining operations. Safety Sci 55:45–52

Li S, Wang K, Li L (2014) Development and application of an extendable model test system for water inrush simulation in subsea tunnel. J Rock Mech Eng 12:2409–2241 **(Chinese)**

Liu Q (2009) A discussion on water inrush coefficient. Coal Geol Explor 37(4):34–42

Lu Y, Wang L (2015) Numerical simulation of mining-induced fracture evolution and water flow in coal seam floor above a confined aquifer. Comput Geotech 67:157–171

Ministry of Coal Industry (2009) Regulations for mine water prevention and control. Beijing Publishing House of Coal Industry, Beijing **(in Chinese)**

Sun W, Zhang S (2015a) Development application of fluid-solid coupling similar material for floor strata and simulation test of water- inrush in deep mining. J Rock Mech Eng S1:2665–2670 **(Chinese)**

Sun W, Zhang S (2015b) Development of floor water invasion of mining influence simulation testing system and its application. J Rock Mech Eng S1:3274–3280 **(Chinese)**

Wang J, Li J, Xu G (2010) Development and application of simulation test system for water inrush from the water-conducting collapse column. J Min Safety Eng 03:305–309 **(Chinese)**

Wang Q, Ye Y, Jiang Y (2011) Simulation on mine water-inrush characteristics of cross roadway based on CFX. Proc Eng 26:759–764

Wang Y, Yang W, Li M, Liu X (2012) Risk assessment of floor water inrush in coal mines based on secondary fuzzy comprehensive evaluation. Int J Rock Mech Min 52:50–55

Wildemeersch S, Brouyère S, Ph. Orban, Couturier J, Dingelstadt C, Veschkens M, Dassargues A (2010) Application of the hybrid finite element mixing cell method to an abandoned coalfield in Belgium. J Hydrol 392:188–200

Wu Q, Zhou W, Pan G, Ye S (2009) Application of a discrete-continuum model to karst aquifers in North China. Ground Water 47(3):453–461

Wu Q, Cui F, Zhao S, Liu S, Zeng Y, Gu Y (2013a) Type classification and main characteristics of mine water disasters. J Chin Coal Soc 38:561–565 **(Chinese)**

Wu Q, Fan S, Zhou W, Liu S (2013b) Application of the analytic hierarchy process to assessment of water inrush: a case study for the No. 17 coal seam in the Sanhejian coal mine, China. Mine Water Environ 32:229–238

Wu Q, Lin Y, Zhou W, Li B, Zhao B, Lin S, Sun W, Zeng Y (2015) Evaluation of water inrush vulnerability from aquifers overlying coal seams in the Menkeqing coal mine, China. Mine Water Environ 34:258–269

Zhang J, Shen B (2004) Coal mining under aquifers in China: a case study. Int J Rock Mech Min 41:629–639

Zhou H, Tang Y, Hu D (2006) Study on coupled penetrating-dissolving model and experiment for salt rock cracks. J Rock Mech Eng 25(5):946–950 **(Chinese)**